PHYSICAL REVIEW B VOLUME 51, NUMBER 22 1 JUNE 1995-II

Computational simulation of type-II superconductivity including pinning phenomena

Qiang Du
Department of Mathematics, Michigan State University, East Lansing, Michigan 48824-1027

Max D. Gunzburger and Janet S. Peterson
Interdisciplinary Center for Applied Mathematics, Virginia Tech, Blacksburg, Virginia 24061-0531

(Received 27 January 1995)

A flexible tool, based on the finite-element method, for the computational simulation of vortex phenomena in type-II superconductors has been developed. These simulations use refined or newly developed phenomenological models including a time-dependent Ginzburg-Landau model, a variable-thickness thin-film model, simplified models valid for high values of the Ginzburg-Landau parameter, models that account for normal inclusions and Josephson effects, and the Lawrence-Doniach model for layered superconductors. Here, sample results are provided for the case of constant applied magnetic fields. Included in the results are cases of flux pinning by impurities and by thin regions in films.

I. INTRODUCTION

We have developed a flexible and robust computational tool that can be used to study a variety of phenomena involving vortices in type-II superconductors. The desirable features of our algorithms and codes are due to the use of the finite-element method for the discretization of the governing system of partial differential equations. Previously[1] we used this method in the context of periodic problems for the Ginzburg-Landau equations. Here, we apply the finite-element methodology to a variety of Ginzburg-Landau based phenomenological boundary value models for type-II superconductivity. The details of the application of the finite-element method to the current settings are very similar to those for the periodic setting and thus we do not elaborate on these here. One may also consult Du, Gunzburger, and Peterson[2,3] and Du[4] for additional theoretical results concerning finite-elements method in superconductivity.

The development of computational tools has been preceded by the development, refinement, and analysis of phenomenological models for superconductivity. An outline of the models that we have studied and which are incorporated into our codes is given as follows. Details may be found in the cited references.

Time-dependent Ginzburg-Landau model.[4,5] Theoretical results have been obtained and finite-element algorithms have been defined, analyzed, and implemented for the well-known time-dependent Ginzburg-Landau model. The codes we have developed can be used to study vortex motion and other phenomena such as the nucleation of vortices at boundaries.

Variable thickness thin-film model.[6] Models for thin films having variable thickness have been developed. Theoretical results have been obtained, and finite-element algorithms have been defined, analyzed, and implemented. Computational simulations showing the effectiveness of thin regions for pinning vortices have been carried out.

Models accounting for normal-superconductor interfaces.[7] Models that can account for normal materials such as impurities or layers coexisting with superconducting materials have been developed and analyzed. Computational simulations showing the effectiveness of normal impurities for pinning vortices have been carried out. The same code has been used to show how the model can be used to study other normal-superconducting interfaces such as Josephson junctions.

Models for high values of κ.[8,9] Simplified models have been studied and analyzed that are valid for large values of the Ginzburg-Landau parameter κ. Computational simulations illustrating the accuracy of the simplified model have been carried out.

Lawrence-Doniach model.[9] The connection between this model for layered superconductors and the anisotropic Ginzburg-Landau model has been rigorously established. Theoretical results have been obtained, and finite-element algorithms have been defined. Preliminary computational simulations have been carried out.

Below, we give some additional details and provide results of computational simulations for the case of constant applied magnetic fields. The results of other simulations involving applied currents and voltages as well as thermal fluctuation effects will be given elsewhere.

II. TIME-DEPENDENT GINZBURG-LANDAU MODEL

The time-dependent Ginzburg-Landau (TDGL) equations were developed by Gor'kov and Eliashberg;[10] our starting point is the version given in Gor'kov and Kopnin.[11] We introduce a length scale l and nondimensionalize the spatial and time coordinates $\mathbf{x}$ and t, the order parameter ψ, the magnetic potential $\mathbf{A}$, and the electric potential Φ according to

$$\mathbf{x}\rightarrow l\mathbf{x},\quad t\rightarrow\frac{\gamma\hbar}{|\alpha|}t,\quad \psi\rightarrow\sqrt{(|\alpha|/\beta)}\psi\ ,$$

$$\mathbf{A}\rightarrow\sqrt{(8\pi\alpha^2 l^2/\beta)}\,\mathbf{A},\quad \text{and}\quad \Phi\rightarrow\frac{|\alpha|}{\gamma e_s}\Phi\ ,$$

respectively, where $e_s=2e$ and m_s are the charge of and

mass, respectively, of the superconducting charge carriers, e is the electron charge, $2\pi\hbar$ is Plank's constant, α and β are the temperature-dependent coefficients appearing in the condensation energy contribution to the Ginzburg-Landau free energy, and γ is a time relaxation parameter. The Ginzburg-Landau coherence length and the London penetration depth are given by

$$\xi=\frac{\hbar}{\sqrt{2m_s|\alpha|}} \quad \text{and} \quad \lambda=\sqrt{(\beta m_s c^2/4\pi|\alpha|e_s^2)} ,$$

respectively, where c is the speed of light. Of course, the Ginzburg-Landau parameter $\kappa=\lambda/\xi$. The most common choices for the length scale are either $l=\xi$ or $l=\lambda$.

In nondimensionalized form, the TDGL equations for the order parameter ψ, magnetic potential $\mathbf{A}$, and electric potential Φ are then given by

$$\frac{\partial\psi}{\partial t}+i\Phi\psi=\psi-|\psi|^2\psi-\left[i\frac{\xi}{l}\nabla+\frac{l}{\lambda}\mathbf{A}\right]^2\psi \quad \text{in } \Omega \tag{1}$$

and

$$-\sigma\left[\frac{\partial\mathbf{A}}{\partial t}+\frac{\lambda\xi}{l^2}\nabla\Phi\right]=\nabla\times\nabla\times\mathbf{A}+\frac{l^2}{\lambda^2}|\psi|^2\mathbf{A}+\frac{i}{2}\frac{\xi}{\lambda}(\psi^*\nabla\psi-\psi\nabla\psi^*) \quad \text{in } \Omega , \tag{2}$$

where Ω denotes the region occupied by the superconductor,

$$\sigma=\sigma_n\frac{2\pi\hbar}{\gamma m_s c^2}\frac{l^2}{\xi^2} ,$$

and σ_n is the normal conductance. We also have the boundary conditions

$$\left[i\frac{\xi}{l}\nabla+\frac{l}{\lambda}\mathbf{A}\right]\cdot\mathbf{n}=0 \quad \text{on } \Gamma \tag{3}$$

and

$$(\nabla\times\mathbf{A})\times\mathbf{n}=\mathbf{H}\times\mathbf{n} \quad \text{on } \Gamma , \tag{4}$$

where $\mathbf{n}$ denotes the unit normal vector of the boundary Γ of Ω and $\mathbf{H}$ denotes the applied field, and the initial conditions

$$\psi(\mathbf{x},0)=\psi_0(\mathbf{x}) \quad \text{in } \Omega \tag{5}$$

and

$$\mathbf{A}(\mathbf{x},0)=\mathbf{A}_0(\mathbf{x}) \quad \text{in } \Omega , \tag{6}$$

where we assume that $\nabla\cdot\mathbf{A}_0=0$ and $|\psi_0(x)|\leq 1$; the latter implies that the magnitude of the initial order parameter does not exceed its value at the superconducting state. Solutions of (1)–(6) are unique only up to a gauge transformation; for problems wherein the applied field $\mathbf{H}$ is constant, we use the gauge choice

$$\mathbf{A}\cdot\mathbf{n}=0 \quad \text{on } \Gamma \quad \text{and} \quad \Phi=0 \quad \text{in } \Omega . \tag{7}$$

The global existence and uniqueness of appropriately defined weak solutions of (1)–(7) have been demonstrated;[5] see also Ref. 12. Additional results include the continuous dependence of the solution on the initial data. Discretization algorithms for the TDGL equations have been developed and analyzed.[4] First, semidiscrete Galerkin finite-dimensional approximations were examined. (Here, by semidiscrete, we mean that only discretization with respect to the spatial variables is considered.) In this case, the convergence of the approximations as the dimension of the approximating spaces tend to ∞ was proved. This result was also specialized to the concrete case of finite-element approximations. The backward Euler based fully discrete approximating scheme and a second-order accurate in time scheme were also considered. In both cases, rigorous error estimates were derived.

These schemes are used in a two-dimensional code we have developed. Spatial discretization is effected using piecewise biquadratic polynomials. Typical results of our computational simulations are given in Figs. 1–3. The Ginzburg-Landau parameter κ is set equal to 20 and the external field H, which points perpendicular to the plane, is set equal to 10. Figure 1 shows the time evolution of the level curves of the magnitude of the order parameter for the phenomena of vortex nucleation at the boundary of the sample. (Increasing time runs from left to right and then top to bottom. Also, for the sake of clarity, we have only plotted the level curves for $|\psi|\leq 0.5$.) The sample is a square having sides equal to 20 coherence lengths. Initial conditions correspond to a perfect superconducting state. Vortices first start to form at the edges and then settle down into the interior. Since the applied field is a constant and there are no external currents or voltages applied to the sample, the vortices approach a steady-state configuration which is depicted in Fig. 2.

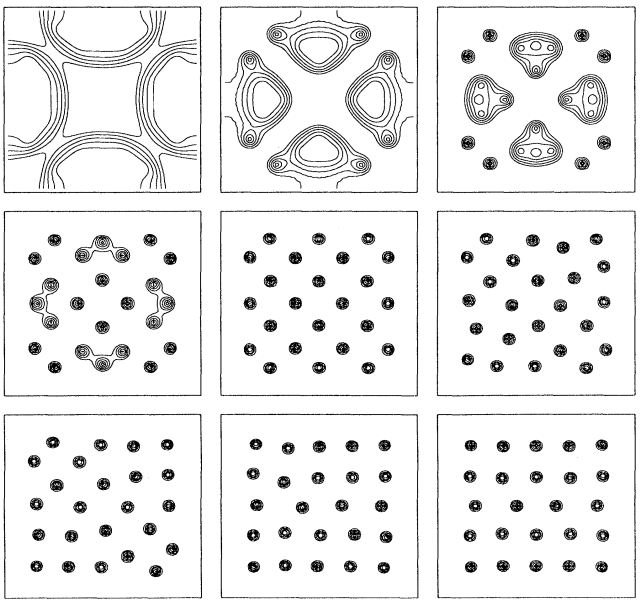

FIG. 1. Time evolution of vortices for a type-II superconductor.

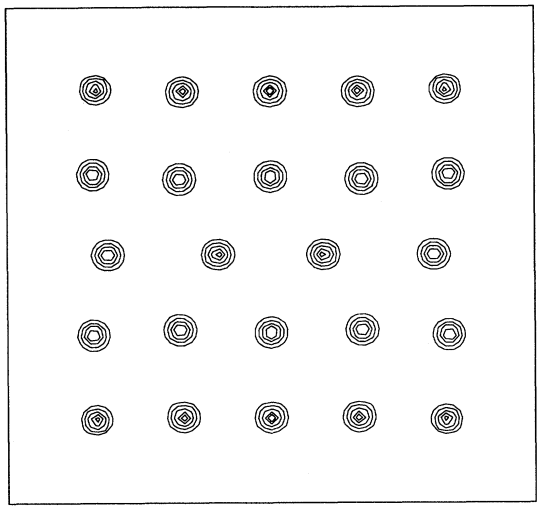

FIG. 2. Steady-state vortex configuration for a type-II superconductor.

The steady-state supercurrent field is given in Fig. 3; one clearly sees the shielding current running along the boundary of the sample, along with the current circulating around each vortex. (For the sake of clarity, we have plotted the current vectors on a coarser grid than that actually used for the computations.)

The TDGL code we have developed forms the basis for the other codes that we use to obtain approximations of solutions of the variants of the Ginzburg-Landau model discussed below. The results obtained from these codes are time accurate so that they can be used to simulate both transient and steady-state phenomena. Elsewhere, we will report on the application of our methodology to problems involving applied currents and voltages and also vortex motions due to temperature fluctuations. We note that all the results presented here were obtained on workstations.

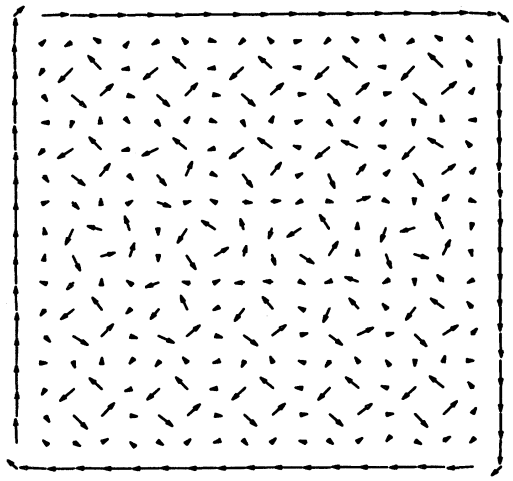

FIG. 3. Steady-state supercurrent distribution for a type-II superconductor.

III. A VARIABLE THICKNESS THIN-FILM MODEL

We now turn to a description of models that have been developed for variable thickness thin films.[6] Variations in thickness can have significant effects on the electromagnetic behavior of the superconductor, e.g., there is evidence that vortices can be trapped within narrow (thin) regions. Thin films of superconducting material are often modeled as two-dimensional objects. The third dimension, i.e., that across the film, is eliminated by an averaging procedure. If the properties of the material, viewed as a three-dimensional object, are homogeneous, and the thickness of the film is invariant with position, then the result of the averaging process will be a two-dimensional model having constant coefficients. One would like to have a two-dimensional model that can account for thickness variations. Any such model would result from an averaging process across the film that varies from point-to-point in the plane of the film, and introduces the variable thickness into the coefficients of the resulting two-dimensional model.

We consider the case where a three-dimensional thin layer in $\mathbb{R}^3$ is symmetric with respect to the (x,y) plane. (Other film geometries can be treated in a similar manner.) The z axis is thus perpendicular to the symmetry plane of the film. Then, the thin-film Ω_ϵ can be defined by

$$\Omega_\epsilon=\{(x,y,z)\in\mathbb{R}^3 | (x,y)\in\Omega_0\subset\mathbb{R}^2,$$
$$z\in[-\epsilon a(x,y),\epsilon a(x,y)]\}\ ,$$

where ϵ is small parameter and $a(x,y)$ is assumed to satisfy $a(x,y)>0$ for all $(x,y)\in\Omega_0$. The constant external field may point in directions other that perpendicular to the center plane of the film, i.e., $\mathbf{H}=(H_1,H_2,H_3)$. The planform of the film is denoted by Ω_0 and its boundary by Γ_0.

We choose the length scale $l=\xi$. Then, to leading order in ϵ, the order parameter satisfies

$$(i\tilde{\nabla}+\tilde{\mathbf{A}}_0)\cdot a(i\tilde{\nabla}+\tilde{\mathbf{A}}_0)\psi_0+a(|\psi_0|^2-1)\psi_0=0 \quad \text{in } \Omega_0 \tag{8}$$

and

$$(i\tilde{\nabla}\psi_0+\tilde{\mathbf{A}}_0\psi_0)\cdot\mathbf{n}=0 \quad \text{on } \Gamma_0\ , \tag{9}$$

where $\tilde{\mathbf{A}}_0=(\tilde{A}_{01},\tilde{A}_{02})$ is a magnetic potential such that $\kappa\nabla\times(\tilde{\mathbf{A}}_0,0)=(0,0,H_3)$ and $\tilde{\nabla}$ denotes the two-dimensional gradient with respect to x and y. Thus, to leading order, the magnetic field is unaffected by the presence of the thin film.

When the film is of uniform thickness, i.e., $a\equiv 1$, the thin-film model of (8) and (9) is identical to a model for superconducting cylinders as the Ginzburg-Landau parameter tends to ∞; see (28) and (29). This means that all superconducting materials, whether type-I or type-II in bulk, behave as type-II superconductors when made into sufficiently thin films.[13–18]

Equations that determine the first-order correction to the magnetic field have also been derived;[6] these are given by

$$\nabla\cdot\mathbf{h}_1=0 \quad \text{and} \quad \nabla\times\mathbf{h}_1=\mathbf{0} \tag{10}$$

everywhere and

$$[\mathbf{h}_1\times\mathbf{k}]_{0-}^{0+}=\mathbf{j}_{s0}\ , \tag{11}$$

where $[\ ]_{0-}^{0+}$ denotes the jump across the plane of the film and where $\mathbf{j}_{s0}$ is the (leading-order) superconducting surface current given by

$$\mathbf{j}_{s0}=-\frac{i}{2}(\psi_0^*\nabla\psi_0-\psi_0\nabla\psi_0^*)-|\psi_0|^2\,\tilde{\mathbf{A}}_0\ .$$

The total field is given by $\mathbf{h}=\mathbf{H}+\epsilon\mathbf{h}_1$.

Various results concerning the solution of the variable thickness thin-film equations (8) and (9) have been derived. In particular, the rigorous connection between solutions of (8) and (9) and solutions of the three-dimensional steady-state Ginzburg-Landau equations has been established. For example, one has the following consistency result. For any $\epsilon>0$, denote by $(\psi_\epsilon, \mathbf{A}_\epsilon)$ the solution of the constant coefficient, three-dimensional, steady-state Ginzburg-Landau equations over the three-dimensional domain Ω_ϵ. Let

$$\bar{\psi}_\epsilon(x,y)=\frac{1}{2\epsilon a}\int_{-\epsilon a}^{\epsilon a}\psi_\epsilon(x,y,z)dz, \quad \forall(x,y)\in\Omega_0$$

and

$$\overline{\mathbf{A}}_\epsilon(x,y)=\frac{1}{2\epsilon a}\int_{-\epsilon a}^{\epsilon a}\mathbf{A}_\epsilon(x,y,z)dz, \quad \forall(x,y)\in\Omega_0\ .$$

Thus, for any $(x,y)\in\Omega_0$, $\bar{\psi}_\epsilon$ and $\overline{\mathbf{A}}_\epsilon$ are the averages across the film of the solutions of the three-dimensional Ginzburg-Landau equations in the film, the latter viewed as a three-dimensional object. Then, the consistency result is the following: the sequence $\{(\bar{\psi}_\epsilon, \overline{\mathbf{A}}_\epsilon)\}$ of solutions of the three-dimensional Ginzburg-Landau equations converges, as $\epsilon\to 0$, to a solution $(\psi_0, \tilde{\mathbf{A}}_0)$ of the variable thickness thin-film equations (8) and (9). Another interesting conclusion that can be drawn from (7) and (8) is that all superconducting materials, whether type-I or type-II in bulk, behave as type-II superconductors when made into sufficiently thin films.[6,13–18]

We have developed a code for determining finite-element approximations to the solution of the variable thickness thin-film equations (8) and (9). Piecewise biquadratic finite-element functions are used. Typical results are given in Fig. 4. Again, we have a square sample with sides equal to 20 coherence lengths; the applied field has magnitude 0.5κ; note from (7) and (8) that, to leading order, the order parameter in a thin film does not depend on κ. In Fig. 4(a), the steady-state vortex configuration is given for a constant thickness thin film; again, we are plotting the level curves of the magnitude of the order parameter. Next, we introduce ten thin regions into the sample; each of these is a square with sides equal to one coherence length. The position of the thin regions is depicted in Fig. 4(b). In each of these regions, the thickness function a is set to 0.1; elsewhere in the sample, $a=1$. The vortices for this configuration are depicted in Fig. 4(c); it is clear that vortices are attracted to thin regions, i.e., they are pinned by these regions. This is even more evident from Fig. 4(d) for which we have superimposed Figs. 4(b) and 4(c).

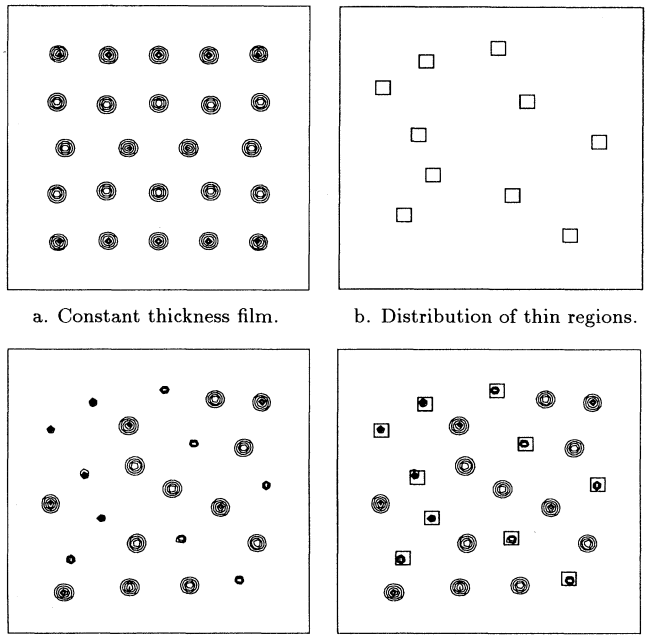

a. Constant thickness film. b. Distribution of thin regions.

c. Variable thickness film. d. Figs. 4b and 4c superimposed.

FIG. 4. Pinning of vortices by thinner regions in a thin film.

To leading order, the magnetic field is given by the applied field. The first-order correction to the magnetic field may be determined from (10) and (11). For the configuration of Fig. 4(a), the first-order correction to the magnetic field above the sample is given in Fig. 5(a). Specifically, that figure depicts the magnetic field in a portion of the half-plane above the horizontal midline of the sample. (Actually, we have scaled fields by κ, i.e., we plot $\mathbf{h}_1/\kappa$.) The scaled total field $\mathbf{h}/\kappa=(0,0,0.5)+\epsilon\mathbf{h}_1/\kappa$ is depicted in Fig. 5(b) for $\epsilon=0.1$. The horizontal midline of the sample is also depicted at the bottom of that figure; thus, the field is depicted in a region that extends

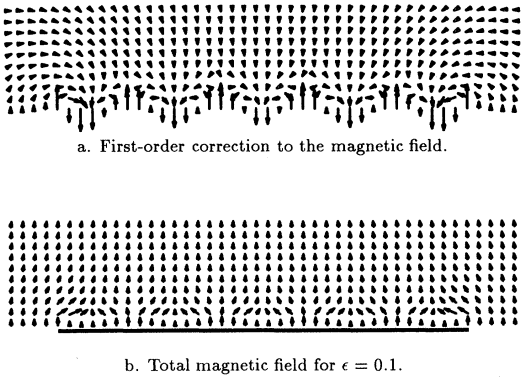

a. First-order correction to the magnetic field.

b. Total magnetic field for $\epsilon = 0.1$.

FIG. 5. Correction and total magnetic field above the vertical midline of the sample.

to the left and right of the sample. One can see in Fig. 5(b) the pinching of the field lines at the vortex cores.

IV. A MODEL ACCOUNTING FOR NORMAL-SUPERCONDUCTING JUNCTIONS

Models that can account for normal-superconducting junctions and normal inclusions are of considerable practical interest. For examples, normal impurities can be used to pin vortices and Josephson junctions consist of thin layers of normal material sandwiched between superconducting materials. A two-parameter model that can account for such situations has been developed; it may be viewed as a generalization of models given in Larkin[19] and Likharev.[20]

To understand the steady-state version of the model, we need to write down the Ginzburg-Landau functional in dimensional form, which, to within a constant additive factor, is given by

$$\mathcal{G}(\psi,\mathbf{A})=\int_\Omega\left[\alpha|\psi|^2+\frac{\beta}{2}|\psi|^4+\frac{1}{2m}\left|\left[i\hbar\nabla+\frac{2e}{c}\mathbf{A}\right]\psi\right|^2+\frac{|\mathbf{h}-\mathbf{H}|^2}{8\pi}\right]d\Omega\ .$$

Here, $\mathbf{h}$ denotes the magnetic field so that $\mathbf{h}=\nabla\times\mathbf{A}$ and $\mathbf{H}$ denotes the applied magnetic field. For a superconducting material, the parameter α changes sign at the critical temperature T_c, with $\alpha<0$ for $T<T_c$ and $\alpha>0$ for $T>T_c$. (The parameter $\beta\geq 0$ always.) In the model, one chooses $\alpha<0$ in the superconducting material and $\alpha>0$ in the normal material. Whenever $\alpha>0$, the role of the parameter β becomes unimportant, so that one can choose $\beta=0$ in the normal material. An arbitrary choice for the mass parameter m in the two materials is allowed for as are different permeabilities μ. Thus, we define a free energy

$$\int_{\Omega_s}\left\{\alpha_s|\psi|^2+\frac{\beta_s}{2}|\psi|^4+\frac{1}{2m_s}\left|\left[i\hbar\nabla+\frac{2e}{c}\mathbf{A}\right]\psi\right|^2+\frac{\mu_s}{8\pi}|\mathbf{h}-\mathbf{H}|^2\right\}d\Omega+\int_{\Omega_n}\left\{\alpha_n|\psi|^2+\frac{1}{2m_n}\left|\left[i\hbar\nabla+\frac{2e}{c}\mathbf{A}\right]\psi\right|^2+\frac{\mu_n}{8\pi}|\mathbf{h}-\mathbf{H}|^2\right\}d\Omega\ ,$$

where Ω_n and Ω_s denote the regions occupied by the normal and superconducting materials, respectively. Minimizers of this functional must satisfy the equations (nondimensionalizations have been introduced and $l=\lambda$ has been chosen)

$$\left[\frac{i}{\kappa}\nabla+\mathbf{A}\right]^2\psi-\psi+|\psi|^2\psi=0\ \text{ in }\Omega_s\ , \tag{12}$$

$$\nabla\times\nabla\times\mathbf{A}=-\frac{i}{2\kappa}(\psi^*\nabla\psi-\psi\nabla\psi^*)-|\psi|^2\mathbf{A}\ \text{ in }\Omega_s\ , \tag{13}$$

$$\frac{1}{m}\left[\frac{i}{\kappa}\nabla+\mathbf{A}\right]^2\psi+\alpha\psi=0\ \text{ in }\Omega_n\ , \tag{14}$$

$$\frac{1}{\mu}\nabla\times\nabla\times\mathbf{A}=-\frac{1}{m}\left[\frac{i}{2\kappa}(\psi^*\nabla\psi-\psi\nabla\psi^*)+|\psi|^2\mathbf{A}\right]\ \text{ in }\Omega_n\ , \tag{15}$$

$$[\mathbf{A}]=\mathbf{0},\quad [\psi]=0\ , \tag{16}$$

$$\left[\mathbf{n}\cdot\frac{1}{m}\left[\frac{i}{\kappa}\nabla+\mathbf{A}\right]\psi\right]=0\ , \tag{17}$$

and

$$\left[\frac{1}{\mu}(\nabla\times\mathbf{A})\times\mathbf{n}\right]=0\ , \tag{18}$$

where $m=m_n/m_s$, $\mu=\mu_n/\mu_s$, $\alpha=m_n\alpha_n/(m_s|\alpha_s|)$, $[\ ]$ denotes the jump across the interface Γ between Ω_s and Ω_n, and $\mathbf{n}$ denotes the unit normal vector of Γ. In general, one has no control over the values of the permeabilities μ_n and μ_s. Likewise, the Ginzburg-Landau parameter κ is fixed by the choice of superconducting material. Thus, there are two constants at one's disposal in defining the model, namely, m and α. The freedom afforded by these two parameters enables the model (12)–(18) to account for a variety of normal-superconducting phenomena. We now describe how the model accounts for some of these. See Chapman, Du, and Gunzburger[7] for details.

For the model of (12)–(18), the order parameter and the supercurrent in the normal region do not vanish; the latter is given by

$$\mathbf{J}=-\frac{1}{m}\left[\frac{i}{2\kappa}(\psi^*\nabla\psi-\psi\nabla\psi^*)+|\psi|^2\mathbf{A}\right]\ \text{ in }\Omega_n\ .$$

Thus, the model can be used to describe the proximity effect.

In one dimension and in the absence of a potential it can be shown that on the superconducting side of a superconducting-normal interface the order parameter satisfies the relation

$$\psi'=-\frac{\kappa\sqrt{\alpha}}{m}\psi\ ,$$

where $(\ )'$ denotes the (normal) derivative. Thus, we retrieve the de Gennes boundary condition[21]

$$\psi' = -\gamma\psi$$

with $\gamma = \kappa\sqrt{\alpha}/m$. The corresponding boundary condition for a superconducting-vacuum interface should be $\psi' = 0$. This boundary condition is recovered from the model (12)–(18) by letting $\alpha \to \infty$ and $m \to \infty$ in such a way that $\sqrt{\alpha}/m \to 0$.

The model (12)–(18) can also account for the de Gennes relations across a Josephson junction.[21] Here, one has a normal region sandwiched between two superconducting regions. Let $(\,)^+$ and $(\,)^-$ denote evaluation of a quantity in the superconducting material at the left- and right-hand interfaces with the normal material. De Gennes then gave the relation

$$\begin{bmatrix} \psi \\ \mathbf{n}\cdot\left[\frac{1}{\kappa}\nabla - i\mathbf{A}\right]\psi \end{bmatrix}^+ = \begin{bmatrix} M_{11} & M_{12} \\ M_{21} & M_{22} \end{bmatrix} \begin{bmatrix} \psi \\ \mathbf{n}\cdot\left[\frac{1}{\kappa}\nabla - i\mathbf{A}\right]\psi \end{bmatrix}^- \tag{19}$$

for the order parameter and its gauge-invariant normal derivative across the junction. Here, the M_{ij} are real and are determined by the particular junction and depend on its thickness, the type of material, etc. De Gennes postulates that for an insulating material M_{11} and M_{22} are close to unity, and M_{12} and M_{21} are small. The junction is symmetric, i.e., has the same type of superconductor on each side of the junction, if and only if $M_{11} = M_{22}$. In this case, de Gennes shows that

$$M_{11}M_{22} - M_{12}M_{21} = 1 \ . \tag{20}$$

Finally, the supercurrent across the junction is given by

$$J = \frac{1}{M_{12}}|\psi^+\psi^-|\sin(\chi^+ - \chi^-) \ , \tag{21}$$

where χ denotes the phase of the order parameter. All of these relations are directly recoverable from the model (12)–(18). In fact, if we assume that the normal layer has thickness d, and that we have different superconductors on each side of the junction, then the model (12)–(18) yields that (19) is satisfied with

$$\begin{aligned} M_{11} &= \cosh(2\kappa d\sqrt{\alpha}) \ , \\ M_{12} &= (m_n/\sqrt{\alpha})\sinh(2\kappa d\sqrt{\alpha}) \ , \\ M_{21} &= (m_{s_2}\sqrt{\alpha}/m_n)\sinh(2\kappa d\sqrt{\alpha}) \ , \\ M_{22} &= m_{s_2}\cosh(2\kappa d\sqrt{\alpha}) \ . \end{aligned} \tag{22}$$

Here, we have nondimensionalized with respect to one of the superconductors, so that m_n and m_{s_2} denote the nondimensionalized masses of the normal material and the other superconductor. Note that the junction is symmetric if and only if $m_{s_2} = 1$, i.e., only if the superconductors on each side of the junction are the same, and that in this case (20) is satisfied. Also, the model yields that the supercurrent in the junction is given by

$$J = \frac{\sqrt{\alpha}}{m_n \sinh(2\kappa d\sqrt{\alpha})}|\psi^+\psi^-|\sin(\chi^+ - \chi^-) \ ,$$

which, using (22), recovers the de Gennes relation (21). Note that, as expected, J decreases exponentially as d increases and as α increases. Furthermore, J also decreases as m_n increases. Since large m_n corresponds to a highly insulating material, this is in agreement with the experimental observation that junctions made from insulating materials need to be thinner than junctions made from metals in order to obtain the same tunneling current.

In summary, it is important to note that the model (12)–(18) recovers all the well-known conditions at the normal-superconducting interfaces, including the de Gennes formula for the tunneling current.

We have developed a biquadratic finite element code for the variable α, variable m model of Eqs. (12)–(18). Some typical computational results obtained from the code are found in Figs. 6–9. For Fig. 6, we have a 20 coherence-length square, $\kappa = 5$ and a perpendicular applied field having magnitude 2.5. In Fig. 6(a) we have the steady vortex configuration for a "pure," i.e., homogeneous, superconducting sample. Next, we introduce ten inclusions of normal material as depicted in Fig. 6(b); each inclusion is a one coherence-length square. In each of these regions, we choose $\alpha = 1$ for Eq. (14). The distribution of vortices for this configuration of normal inclusions is given in Fig. 6(c); Figs. 6(b) and 6(c) are superimposed in Fig. 6(d). Clearly, the normal inclusions have attracted, i.e., pinned, vortices.

In Fig. 7 we examine a Josephson-junction-type configuration. Figure 7(a) is for the identical set of parameters as Fig. 6(a). Next, we introduce a thin vertical strip of normal material, with $\alpha = 1$ in (14), as depicted in Fig. 7(b); the width of the strip is 0.2 coherence lengths. The resultant vortex distribution is depicted in Fig. 7(c); Figs. 7(b) and 7(c) are superimposed in Fig. 7(d); clearly

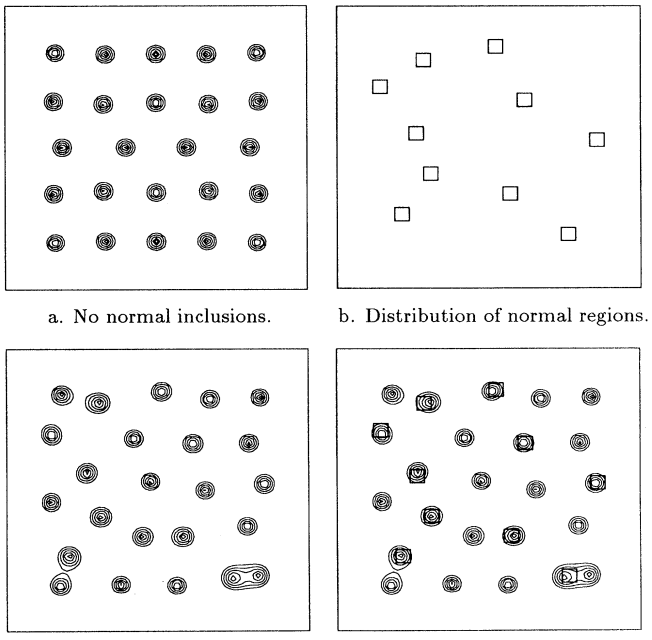

a. No normal inclusions. b. Distribution of normal regions.

c. Sample with normal inclusions. d. Figs. 6b and 6c superimposed.

FIG. 6. Pinning of vortices by normal inclusions.

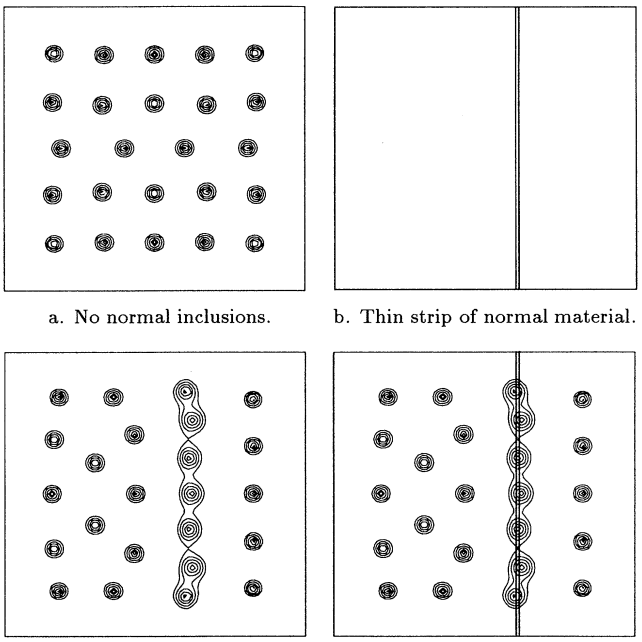

a. No normal inclusions. b. Thin strip of normal material.

c. Josephson junction type sample. d. Figs. 7b and 7c superimposed.

FIG. 7. Vortices in a Josephson-junction-type configuration.

the thin normal strip has attracted vortices. Figure 8 gives the time evolution of the vortices up to the steady state. Figure 9 gives the steady-state supercurrent distribution in the sample. Note how part of the shielding current and the current circulating around each of the seven vortices attracted to the strip pass, i.e., tunnel, through the normal strip.

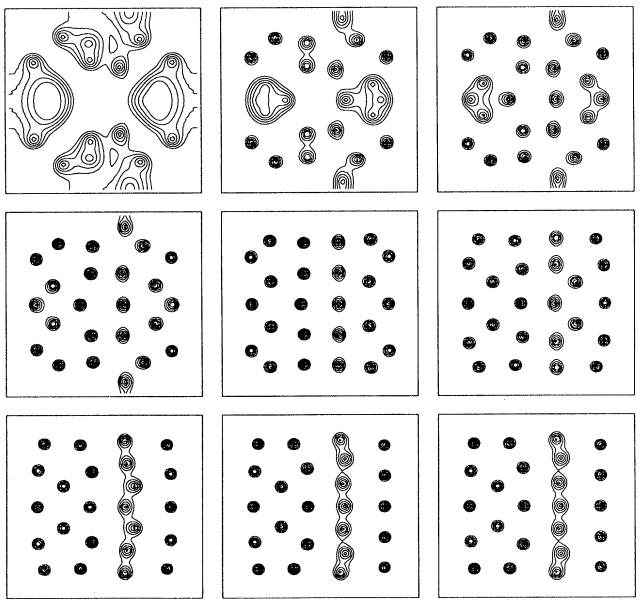

FIG. 8. Time evolution of vortices in a Josephson-junction-type configuration.

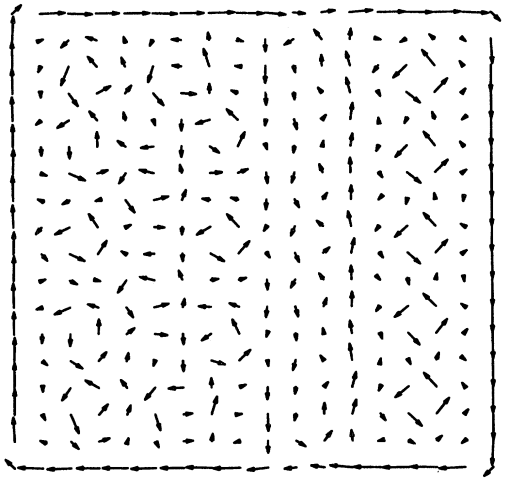

FIG. 9. Current distribution in a Josephson-junction-type configuration.

V. A SIMPLIFIED MODEL VALID FOR LARGE VALUES OF κ

Superconductors are largely characterized by the value of the Ginzburg-Landau parameter κ. The recently discovered high critical temperature superconductors are known to have values of κ in excess of 50. Thus, for technological reasons, there is interest in exploring the behavior of superconductors in the limit of large κ. For the same reasons, high magnetic fields are also of interest. Simplified models of the Ginzburg-Landau type that are valid in the limit of high κ and high applied fields have been developed and analyzed.[8] The discussion below is in the context of the homogeneous, isotropic, Ginzburg-Landau model. Analogous simplifications to order models for superconductivity such as the anisotropic Ginzburg-Landau and Lawrence-Doniach models for layered high critical temperature superconductors have also been effected.[9]

It is assumed that the (nondimensionalized) applied field $\mathbf{H}=\kappa\mathbf{H}_0$, where $\mathbf{H}_0$ is independent of κ. Note that this does not imply that $|\mathbf{H}|$ is near the upper critical field $H_{c2}=\kappa$; for example, one could take $|\mathbf{H}_0|=1/2$. To derive the model, one formally expands the order parameter and magnetic potential in powers of κ:

$$\psi=\sum_{j=0}\frac{1}{\kappa^{2j}}\psi_j \quad \text{and} \quad \mathbf{A}=\kappa\sum_{j=0}\frac{1}{\kappa^{2j}}\mathbf{A}_j \tag{23}$$

and then substitutes these expansions into the full steady-state Ginzburg-Landau equations. Equating powers of κ yields, to leading order, the system for $\mathbf{A}_0$:

$$\nabla\times\nabla\times\mathbf{A}_0=\mathbf{0} \quad \text{in } \Omega \text{ and } \Omega_e\ , \tag{24}$$

$$[\mathbf{A}_0\times\mathbf{n}]=\mathbf{0} \quad \text{on } \Gamma\ , \tag{25}$$

$$[(\nabla\times\mathbf{A}_0)\times\mathbf{n}]=\mathbf{0} \quad \text{on } \Gamma\ , \tag{26}$$

and

$$\nabla\times\mathbf{A}_0\rightarrow\mathbf{H}_0 \quad \text{as } |\mathbf{x}|\rightarrow\infty \tag{27}$$

and the system for ψ_0:

$$(i\nabla + \mathbf{A}_0)^2\psi_0 - \psi_0 + |\psi_0|^2\psi_0 = 0 \quad \text{in } \Omega \,, \tag{28}$$

and

$$\mathbf{n}\cdot(i\nabla + \mathbf{A}_0)\psi_0 = 0 \quad \text{on } \Gamma \,, \tag{29}$$

where Ω denotes the region occupied by the superconducting material, Ω_e is the region external to the superconductor, and Γ is the boundary of the superconductor. Governing systems for the corrections $\mathbf{A}_1$ and ψ_1 have also been derived.[8]

Note that the system (24)–(27) for $\mathbf{A}_0$ is uncoupled from the system (28) and (29), i.e., one may solve the former set of equations for $\mathbf{A}_0$ and then use this solution in the latter set in order to determine ψ_0. Furthermore, the system (24)–(27) implies that, to leading order, the magnetic potential is exactly the same as that would be obtained if the superconducting sample were not present. In many cases, these equations may be easily solved. Thus, the main task to be performed in solving the high-κ, high-field equations is to solve (28) and (29) for the leading-order term ψ_0 in the order parameter. This tremendous simplification, e.g., uncoupling, is not possible with the full Ginzburg-Landau model for which the order parameter and magnetic potential are fully coupled.

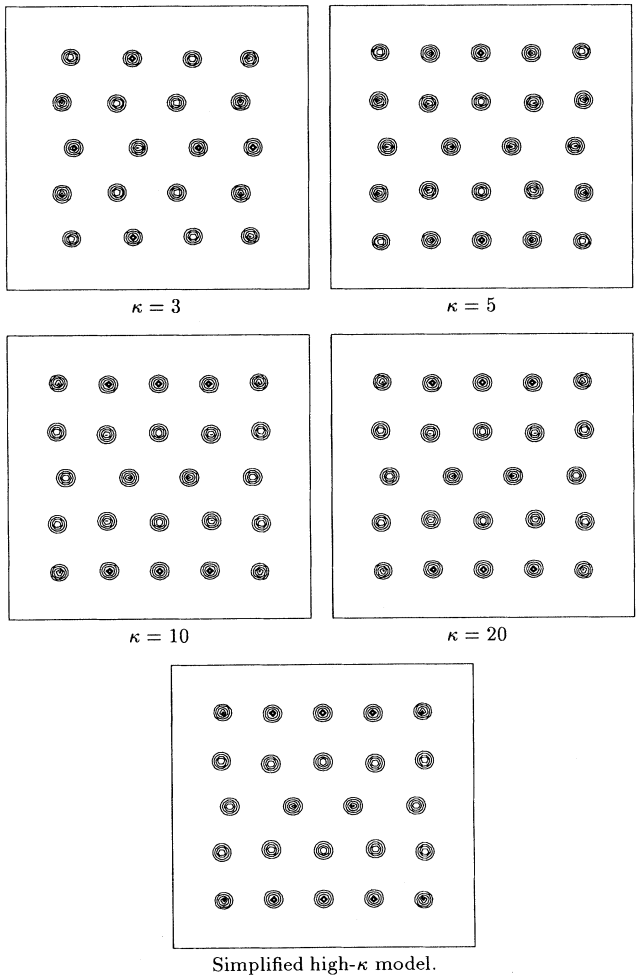

FIG. 10. Vortices for different values of κ and for the simplified high-κ model.

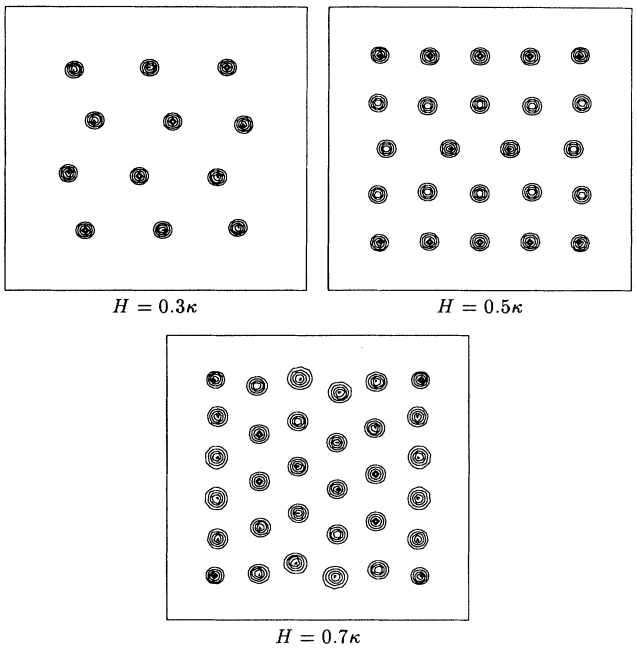

FIG. 11. Effect of magnetic-field strength on the distribution of vortices.

On the theoretical side, it has been shown that as $\kappa \to \infty$, solutions of the full Ginzburg-Landau equations converge to solutions of the leading-order equations (24)–(29). It can actually be shown that the convergence is quadratic, i.e., that $\kappa^{-1}\mathbf{A}_\kappa - \mathbf{A}_0 = O(\kappa^{-2})$ and $\psi_\kappa - \psi_0 = O(\kappa^{-2})$ as $\kappa \to \infty$, where $(\psi_\kappa, \mathbf{A}_\kappa)$ denotes the solution of the full Ginzburg-Landau equations for a

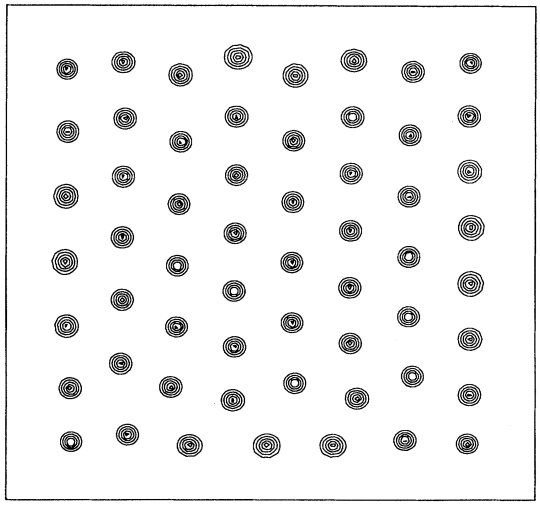

FIG. 12. Vortex distribution in a 30 coherence-length square sample.

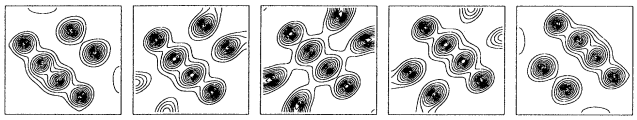

FIG. 13. Vortices in a five-layer square superconductor.

given value of κ. This provides partial justification for the expansions (23) in terms of powers of $1/\kappa^2$.

We have developed a biquadratic finite-element code for finding solutions of the simplified equations (28) and (29). Here, in Fig. 10, we compare results obtained using this code with the results found by using our code for the full, coupled, Ginzburg-Landau equations. As in the previous figures, the sides of the square superconducting samples are of length equal to 20 coherence lengths. The nondimensional applied field is perpendicular to the sample and has magnitude equal to $\kappa/2$. The plots labeled with finite values of κ were obtained from the full Ginzburg-Landau model with the indicated values of κ. The plot labeled with an infinite value of κ was obtained using the simplified model (24)–(29). It is evident from the plots that there is very little difference between the results for the full Ginzburg-Landau equations for values of $\kappa \geq 5$, and that these are also indistinguishable from the results obtained using the leading-order equations. Thus, it seems that the simplified model (24)–(29) yield accurate approximations to solutions of the full Ginzburg-Landau model even for moderate values of κ and of the applied field. In Fig. 11, the effect of increasing applied fields are examined for the simplified model; again a 20 coherence-length square sample is used; the applied field has magnitude equal to 0.3κ, 0.5κ, and 0.7κ for Figs. 11(a), 11(b), and 11(c), respectively. We see that as the applied field increases, more vortices appear. In Fig. 12 we see the effect of increasing the size of the box; now the square sample has sides equal to 30 coherence lengths; the applied field has magnitude $\kappa/2$. Comparing with the 20 coherence-length sample at the same field value [Fig. 11(b)], we see that many more vortices are present. Also, the hexagonal pattern of the vortex lattice is clearly evident away from the boundary of the sample.

VI. THE LAWRENCE-DONIACH MODEL

One of the features of high-T_c superconductors is their layered structure, comprising of alternating layers of superconducting and non- (or weakly) superconducting materials. In planes parallel to the layers, the material is isotropic. However, there is a strong anisotropy present when one compares material properties parallel and perpendicular to the layers. The homogeneous, isotropic Ginzburg-Landau model cannot account for the anisotropy of layered superconductors. In its place, alternative models have been proposed. One of these is the *ansiotropic Ginzburg-Landau model* or *effective-mass model*[22,23] introduced by Ginzburg in 1952. In this model, the effects of the microscopic layered structure are averaged out so that the anisotropic nature of the material appears only in the form of a mass tensor with unequal principal values. The model itself is only a slight variant of the Ginzburg-Landau model. Another model for layered superconductors is the *Lawrence-Doniach model*.[24–26] In this model, the material is treated as a stack of superconducting planes, each pair of which is separated by a vacuum or insulating material. Furthermore, in this model, the coupling between the superconducting planes is similar to that which occurs in a Josephson junction.

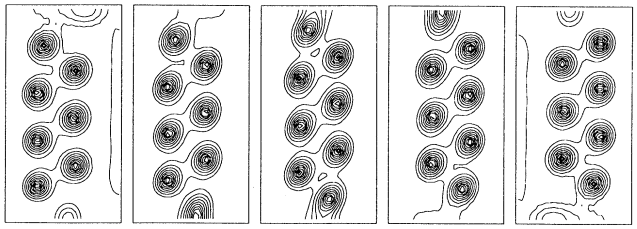

FIG. 14. Vortices in a five-layer rectangular superconductor.

The anisotropic Ginzburg-Landau and Lawrence-Doniach models have been analyzed to show, for example, that appropriately defined free-energy functionals have minimizers in suitable function spaces.[9] The connection between the two models has also been rigorously established. Specifically, it has been rigorously shown that minimizers of the Lawrence-Doniach equations converge, as the interlayer spacing tends to zero, to a solution of the anisotropic Ginzburg-Landau equations. Simplified versions of both models that are valid for high values of κ and applied fields of $O(\kappa)$ have also been derived.

We have developed biquadratic finite-element codes for the Lawrence-Doniach model. These codes take advantage of the simplifications that can be effected for high values of κ so that, notwithstanding the three dimensionality of the model, it can be run on workstations. Here, we present some preliminary results obtained using our Lawrence-Doniach code. In Fig. 13, we have level curve plots of the magnitude of the order parameters for a five-layer superconducting sample. Each layer is a square having sides of length equal to 13 in-layer coherence lengths. The applied field is given by (0.35, 0.35, 0.35) so that it is tilted with respect to the direction perpendicular to the layers. In Fig. 14 a similar plot is given for a five-layer sample for which each layer is a 10 coherence-length by 20 coherence-length rectangle and the applied field is given by (0.4, 0.2, 0.4). In these figures the vortices shift and turn to try to align themselves with the applied magnetic field.

ACKNOWLEDGMENTS

This work was supported by the Department of Energy under Grants No. DE-FG02-93ER25172 for Q. D. and DE-FG05-93ER25175 for M. G. and J. P.

[1]Q. Du, M. Gunzburger, and J. Peterson, Phys. Rev. B **46**, 9027 (1992).
[2]Q. Du, M. Gunzburger, and J. Peterson, SIAM Rev. **34**, 54 (1992).
[3]Q. Du, M. Gunzburger, and J. Peterson, Numer. Math. **64**, 85 (1993).
[4]Q. Du, Comput. Math. Appl. **27**, 119 (1994).
[5]Q. Du, Appl. Anal. (to be published).
[6]J. Chapman, Q. Du, and M. Gunzburger, Z. Agnew. Math. Phys. (to be published).
[7]J. Chapman, Q. Du, and M. Gunzburger, Eur. J. Appl. Math. (to be published).
[8]J. Chapman, Q. Du, M. Gunzburger, and J. Peterson, Adv. Math. Sci. Appl. (to be published).
[9]J. Chapman, Q. Du, and M. Gunzburger, SIAM J. Appl. Math. **55**, 156 (1995).
[10]L. Gor'kov and G. Éliashberg, Sov. Phys. JETP **27**, 328 (1968).
[11]L. Gor'kov and N. Kopnin, Sov. Phys. JETP **38**, 195 (1974).
[12]Z. Chen, K.-H. Hoffman, and J. Liang, Math. Meth. Appl. Sci. **16**, 855 (1993).
[13]G. Lasher, Phys. Rev. **154**, 345 (1967).
[14]J. Livingston and W. Desoro, in *Superconductivity,* edited by R. Parks (Marcel Dekker, New York, 1969), p. 1235.
[15]K. Maki, Ann. Phys. (N.Y.) **34**, 363 (1965).
[16]M. Tinkham, Phys. Rev. **129**, 2413 (1963).
[17]M. Tinkham, Rev. Mod. Phys. **36**, 268 (1964).
[18]M. Tinkham, *Introduction to Superconductivity* (McGraw-Hill, New York, 1975).
[19]A. Larkin, Sov. Phys. JETP **31**, 784 (1971).
[20]K. Likharev, Rev. Mod. Phys. **51**, 101 (1979).
[21]P. de Gennes, *Superconductivity in Metals and Alloys* (Benjamin, New York, 1966).
[22]R. Klemm and J. Clem, Phys. Rev. B **21**, 1868 (1980).
[23]D. Tilley, Proc. Phys. Soc. London **85**, 1177 (1965).
[24]W. Lawrence and S. Doniach, in *Proceedings 12th International Conference of Low Temperature Physics,* edited by E. Kanda (Academic Press of Japan, Kyoto, 1971), p. 361.
[25]L. Bulaevskii, Sov. Phys. JETP **37**, 1133 (1973).
[26]R. Klemm, A. Luther, and M. Beasley, Phys. Rev. B **12**, 877 (1975).